Large resistance decrease around 90–160 K in sputtered Xe-doped Y-Ba-Cu-O thin films on Si substrates

Kazuhiro Hatanaka and Katsuhiro Yokota
Faculty of Engineering, Kansai University, Suita, Osaka, 564, Japan
(Received 30 May 1996; revised manuscript received 27 March 1997)

A resistance decrease of about five orders of magnitude around 90–160 K has been observed in Xe-doped $YBa_{1.5}Cu_{6.3}O_x$, Xe-doped $YBa_{1.5}Cu_{3.7}O_x$, and Xe-doped $YBa_{1.5}Cu_{2.2}O_x$ thin films. These films were deposited on unheated (100)Si substrates by Xe ion-beam sputtering and annealed in an oxygen flow at 100–500 °C for 24 h. The resistance decrease was measured reproducibly for all samples except 500 °C-annealed films even after exposure to atmosphere for two years. The x-ray diffraction pattern study revealed that the films mainly contain $YBa_2Cu_3O_{6.8}$ lattices having compressed *a*-*b* lattice planes and an expanded *c*-axis bond length and $YBa_2Cu_3O_6$ lattices. The presence of xenon-oxygen bonds in the films was determined by x-ray photoelectron spectroscopy. The resistivities first increased with decreasing temperature, exhibited a maximum value at 200–260 K, then exponentially decreased and reached very low resistivities at 95–130 K.
[S0163-1829(97)00833-3]

I. INTRODUCTION

Anomalous resistance behavior has been reported for $YBa_2Cu_3O_x$ (Y-Ba-Cu-O) materials,[1–3] immediately after the discovery of the 90 K phase by Wu *et al.*[4] A sharp resistance decrease at 164 K in low-oxygen content Y-Ba-Cu-O bulk samples has been reported by Naraya *et al.*[2] A resistance decrease at 240 K in the $Y_5Ba_6Cu_{12}O_x$ film has been reported by Chen *et al.*[3] The resistance decreases may lead to the possibility of a higher T_c in Y-Ba-Cu-O superconductors. The materials with higher resistance transition temperatures, however, are reported to exhibit a higher degree of instability with processing variables, particularly temperature cycling during superconductivity measurements. The samples are prepared by a long oxygenation process at low temperature, in addition to the conventionally applied high-temperature oxygen anneal. Ma *et al.*[5] reported an anomalous resistance transition between 160–200 K in $Y_5Ba_6Cu_{12}O_x$ films formed by rapid thermal annealing (RTA) of the $Cu/BaO/Y_2O_3$ layered structures. The films mainly contain the $YBa_3Cu_3O_x$ (Y133) phase and were polycrystals with grain sizes of a few μm. The resistance decrease was stable and reproducible for the resistance measurements that could be repeated more than ten times without reoxygenation.

We report an observed resistance decrease of about five orders of magnitude around 90–160 K in Xe-doped $YBa_{1.5}Cu_{2.2}O_x$ (Xe-Y2), Xe-doped $YBa_{1.5}Cu_{3.7}O_x$ (Xe-Y4), and Xe-doped $YBa_{1.5}Cu_{6.3}O_x$ (Xe-Y6) thin films. The films were formed on (100)Si substrates by Xe ion-beam sputtering and annealed at low temperature for 24 h. The resistance decrease was stable and reproducible even for the films even after exposure in air at room temperature for two years. The film preparation is different from conventional thin film preparation that requires high-temperature oxygen anneal and high substrate temperature deposition.

II. EXPERIMENT

A single-target ion-beam sputtering technique is used to deposit a series of about 110 nm thick films on unheated chemically cleaned (100)Si substrates. The deposition system consists of a stainless-steel chamber, pumped to high vacuum using a 300 *l*/s turbo-molecular pump. The attainable background pressure (without a system bake-out) is in the low 10^{-7} Torr range. The Xe ion beam is incident at 45° from the target normal. The substrate is positioned such that its center is at a 40° angle with respect to the target normal. The ion source-to-target distance is about 5 cm and the target-to-substrate distance is nearly 7 cm. A low-power (1600 eV, 11 mA) Xe ion-beam is focused against 6 cm diameter Y-Ba-Cu-O targets. Under these beam conditions, the deposition rate is low (12 nm/min). The sputtering power used is fairly low (16 W), so excessive target heating is avoided (the target is not water cooled). The substrate temperature reaches about 70 °C due to radiative heating from the ion source and target. A xenon gas flow of 1 SCCM (SSCM denotes cubic centimeter per minute at STP), added to the ion source during deposition, results in a pressure of 2×10^{-3} Torr in the chamber. The chamber is backfilled with 1 atm of oxygen after deposition. The films then are left in the chamber for 24 h. Transformation to the superconducting phase requires a post-deposition anneal treatment. The annealings of the films are performed in flowing oxygen gas at 100–500 °C for 24 h.

The preparation of the target used was as follows. We used high-purity powders of yttrium oxalate, barium carbonate, and copper carbonate and mixed them in the proper proportions. The mixture was calcified in oxygen gas flow at 950 °C for 2 h. Six cm diameter and 3 mm thickness pressed pellets were formed and sintered in oxygen at 950 °C for 2 h. The composition of the target disks is shown in Table I.

Analysis of the film composition was performed using Rutherford backscattering spectrometry (RBS). A 1.5 MeV He ion-beam energy was used, with the detector positioned at a 165° scattering angle. Uncertainty in the determined compositions cannot be smaller than about 5%. Structural characterization of the post-deposition-annealed films was performed using x-ray diffraction. The diffraction angle was accurately measured within $\frac{1}{64}$°. The chemical-bond state of

TABLE I. The cation composition in as-deposited Xe-doped Y-Ba-Cu-O films.

Name	Target comp. Y:Ba:Cu	Film composition				
		Y	Ba	Cu	Xe	O
Xe-Y2	1:3:3	1 ± 0.05	1.5 ± 0.08	2.2 ± 0.1	0.18 ± 0.04	9.0 ± 0.5
Xe-Y4	1:3:5	1 ± 0.05	1.5 ± 0.08	3.7 ± 0.2	0.15 ± 0.03	9.7 ± 0.5
Xe-Y4	1:3:5	1 ± 0.05	1.5 ± 0.08	6.3 ± 0.3	0.16 ± 0.03	11 ± 0.6

each element was analyzed in vacuum using x-ray photoelectron spectroscopy (XPS). For high-resolution XPS, monochromatic Mg $k\alpha$ (1353.6 eV) radiations were used as the x-ray source. Sputtering using an argon ion etching gun is necessary to investigate the inner side of the films. The energy resolution is estimated to ~ 1 eV.

The resistivity was measured for thin films with dimensions of $10\times5\times0.00011$ mm^3 on Si substrates using a four-point technique and for thin films with dimensions of $7\times7\times0.00011$ mm^3 using the van der Pauw technique. During the measurements, the sample was kept in a vacuum (10^{-5} Torr). Thin Au films were deposited on both ends of the film through a mask with an area of 0.5×5 mm^2 to make ohmic contacts for electric current. Two thin Au pads with an area of 0.2 mm^2 were deposited to make ohmic contact for potential difference measurement. The separation between the two electrodes was 3 mm. The current applied in the measurement was 0.2 mA, and voltage was read with an uncertainly of $\pm1.3\,\mu$V, corresponding to $\pm5\times10^{-7}\ \Omega$ cm. Samples were cooled in a cryostat, with resistance and temperature data obtained during cooling or warming using a computer-controlled system. The rate of temperature warming was in a range of 1–10 K/min. The sample temperature was measured using a copper-constantan thermocouple, welded to the dummy sample adjoining the sample. The temperatures were calibrated with an accuracy of 2 °C. The measured samples were kept in conventional plastic cases in a desk in our laboratory room where the humidity was 40–80 % and the temperature was 8–32 °C.

The ac magnetic susceptibility of the films with dimensions of $10\times10\times0.00041$ mm^3 on Si substrates was obtained by measuring the frequency change of an oscillator with 1 007 111.6 Hz due to the transition from a normal state to a superconducting state. The frequency change Δf is proportional to the inductance change of an air core copper coil (210 μH):[6] $\Delta L=-2L(\Delta f/fo)$. The sample film was located in the center of the air core copper coil. The inductance change due to setting the film in the air core copper coil can be calculated as follows: $\Delta L/L=1/\{1+(d/l)/[1+(s/S)\chi]\}$, where d is the film thickness, l is the height (2.5 cm) of the air core copper coil, s is the surface area of the film, S is the cross section (1.77 cm^2) of the air core copper coil, and χ is the real part of the ac magnetic susceptibility of the film. The ac magnetic susceptibility of the films, thus, can be calculated as follows: $\chi\doteq(S/s)[(1/2)(d/l)(fo/\Delta f)-1]$, since $\Delta f/fo\ll1$. The oscillator containing the air core copper coil was located in an electromagnetic shield box surrounded by copper plates of 20 mm thickness. The frequency stability of the oscillator was below ±2 Hz/10 h at 300 ± 0.1 K. The frequency changes were recorded using a high-resolution nine digit counter as a function of temperature. The amplitude of the ac field was 0.7 Oe. The box was evaluated and immersed into a Dewar filled with liquid nitrogen. The sample temperature attained equilibrium at 86.6 K because of heat loss due to the thermal conduction of exhausting pipes. The box was then left in the Dewar boiled out liquid nitrogen. The sample temperature increased at much smaller rates. We failed to precisely control the sample temperature using a computer because the electromagnetic shield box had a larger heat capacity.

III. EXPERIMENTAL RESULTS AND DISCUSSION

A. Composition and structure

A typical RBS spectrum of an as-deposited Xe-Y6 on Si substrates is shown in Fig. 1. Compositions in the as-deposited films are determined using a RBS simulation fitting and the film thickness measured using an interference microscope. The compositions in the as-deposited films are shown in Table I. The stoichiometric cation transfer from the target to the film was unsuccessful. A cation compositional difference between the target and the film arises because the deposition rate was higher than 3 nm/min, required for the stoichiometric transfer.[7,8] The copper composition in the films is proportion to that in the target: it was about 70% of the copper composition in the targets. The barium composition in the films was half that in the targets, independent of the copper composition. Yttrium transferred from the target to the film was more than the other cations. The xenon composition was approximately the same on all the films within the uncertainty of the measurement. The oxygen composition increased slightly with increasing the copper composition in the target. However, the analysis of the oxygen composition may have an uncertainty more than that of cation composi-

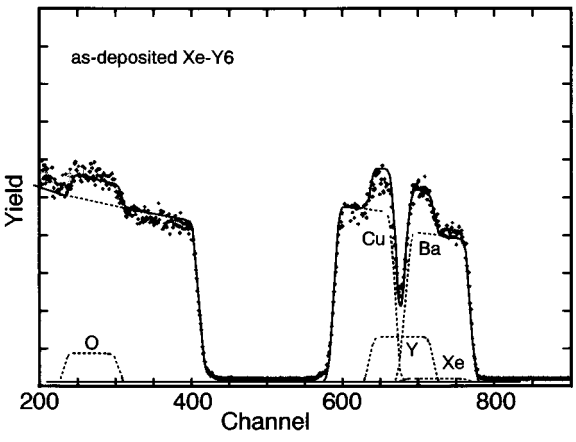

FIG. 1. The RBS spectrum of an as-deposited Xe-Y6 film on Si.

TABLE II. Oxygen and xenon compositions normalized by Y in Xe-doped Y-Ba-Cu-O films annealed in oxygen flow for 24 h.

Anneal temp.	Species	Xe-Y2	Xe-Y4	Xe-Y6
100 °C	O	9.2±0.5	13±0.7	15±0.8
	Xe	0.16±0.03	0.14±0.03	0.14±0.03
150 °C	O	9.2±0.5	13±0.7	15±0.8
	Xe	0.16±0.03	0.13±0.02	0.12±0.02
200 °C	O	8.7±0.4	12±0.6	14±0.7
	Xe	0.15±0.03	0.14±0.03	0.14±0.02

tions because oxygen has scattering cross section smaller than the substrate element, silicon, and the oxygen signal is located in a large background produced by silicon. The scattering cross section of the element with an atomic number of 8 is only $\frac{4}{49}$ [obtained from $(\frac{8}{28})^2$] of that of silicon. Table II shows the oxygen and xenon compositions in annealed films. The oxygen composition increased with increasing the copper composition. The annealed films had approximately the same cation composition as that in the as-deposited films.

The films were polycrystalline with grain sizes of 0.5–3 mm obtained by scanning electron microscopy and an average thickness of 110 nm. The x-ray diffraction pattern for Xe-Y4 is shown in Fig. 2. The diffraction patterns were indexed on the basis of the known Y-Ba-Cu-O structures. The films were composed of semiconducting $YBa_2Cu_3O_6$ and superconducting $YBa_2Cu_3O_{6.8}$. The diffraction patterns for other annealed films were similar to that for Xe-Y4 as shown in Fig. 2. The lattice parameters of Y-Ba-Cu-O were calculated by fitting the x-ray diffraction peak positions. Table III shows the value of $\delta L=(L_X-L_A/L_X)$ for the $YBa_2Cu_3O_{6.8}$ phase. Here, L_X is the measured lattice parameter and L_A is the lattice parameter in the American Society for Testing Materials (ASTM) data. The value of $(b-a)$, as a parameter exhibiting the orthorhombic distortion, is represented in this table for later discussion. The a and b lattice parameters are

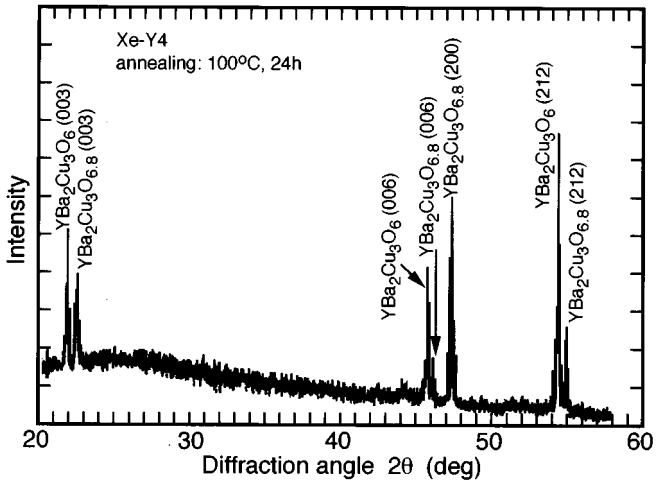

FIG. 2. The x-ray-diffraction patterns of Xe-Y4 film annealed at 100 °C for 24 h.

slightly smaller than the ASTM values for $YBa_2Cu_3O_{6.8}$, and the c lattice parameter is slightly larger. The absolute values of δa and δb decrease with increasing annealing temperature and the value of dc decreases. The films without xenon have the same lattice parameter as the ASTM file. Thus the compression of the a-b lattice planes and the expansion of the c-axis bond length were a result of doping xenon into $YBa_2Cu_3O_{6.8}$. The lattice parameters for $YBa_2Cu_3O_6$ in the annealed films, however, are the same as that in the ASTM file.

B. Chemical bonds

The chemical properties of the bonds were studied using XPS each time a layer of about 14 nm was removed from the sample surface by argon ion-beam sputtering in the spectrometer chamber. Figure 3 shows the XPS results for copper and oxygen in annealed Xe-Y2, Xe-Y4, and Xe-Y6 films. The annealed films exhibit the Cu_{2p} peak and its satellite

TABLE III. Values of $(L_x-L_{\mathrm{ASTM}})/L_x$ for $YBa_2Cu_3O_{6.8}$ in Xe-doped Y-Ba-Cu-O films annealed in oxygen flow for 24 h, where L_x is the lattice parameter for $YBa_2Cu_3O_{6.8}$ and L_{ASTM} is the ASTM standard: $a=3.8214$ Å, $b=3.8877$ Å, and $c=11.693$ Å.

Anneal temp.	parameter	Xe-Y2	Xe-Y4	Xe-Y6
100 °C	a (%)	−0.410±0.0001	−0.397±0.0003	−0.277±0.0004
	b (%)	−2.98±0.001	−2.83±0.002	−1.82±0.001
	c (%)	0.561±0.0002	0.434±0.0002	0.342±0.0001
	$(b-a)$ (Å)	−0.03±0.002	−0.03±0.005	0.01±0.002
150 °C	a (%)	−0.408±0.0001	−0.357±0.0002	−0.199±0.0003
	b (%)	−2.89±0.001	−2.45±0.003	−1.67±0.002
	c (%)	0.352±0.0003	0.558±0.0002	0.352±0.0002
	$(b-a)$ (Å)	−0.03±0.002	−0.01±0.003	0.01±0.001
200 °C	a (%)	−0.377±0.0002	−0.356±0.0003	−0.189±0.0002
	b (%)	−1.92±0.001	−1.83±0.001	−1.67±0.003
	c (%)	0.382±0.0003	0.352±0.0004	0.362±0.0002
	$(b-a)$ (Å)	−0.01±0.003	−0.01±0.002	0.01±0.001

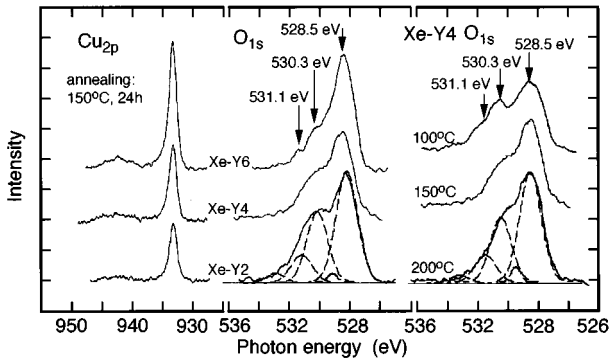

FIG. 3. X-ray photoelectron spectrum for copper and oxygen in the Xe-Y2, Xe-Y4, and Xe-Y6 films.

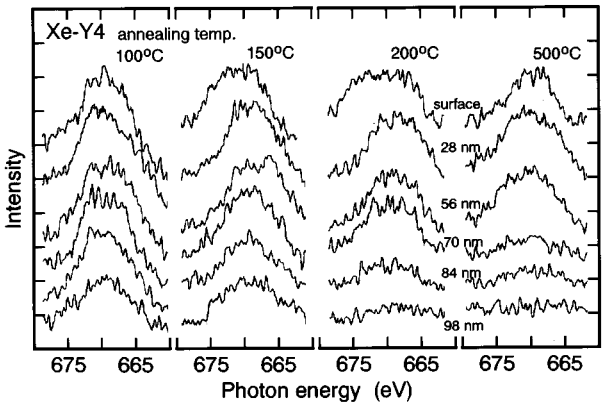

FIG. 4. The Xe $3d_{5/2}$ spectra vs photon energy graphs of the Xe-Y4 films annealed at 100–500 °C for 24 h. The dashed lines shows components separated by curve fitting with a combination of Gaussian and Lorenzian distributions.

peak having binding energies with centroids at 933.2 and 942.3 eV, respectively. The presence of the satellite peak in the Cu_{2p} spectrum shows that the oxidation state of copper is Cu^{2+}. This is an indication of the formation of superconducting Y-Ba-Cu-O or CuO in the films.

The superconducting Y-Ba-Cu-O bulk shows the O 1*s* spectra consisting of two distinct peaks, having binding energies with centroids at 529.5 and 531.1 eV.[9] In degraded samples exposed to air for a long time, the major peak is usually the higher binding energy peak at 531 eV. The lower binding energy component at 529.5 eV arises from the oxygen in the superconducting Y-Ba-Cu-O lattice.[9] However, the Xe-doped Y-Ba-Cu-O films (Xe-Y2, Xe-Y4, and Xe-Y6) can be fitted to distinct O 1*s* peaks, having binding energies with centroids at 528.5, 529.3, 530.3, 531.1, and 533 eV as shown by the dashed lines in Fig. 3. These components are separated by curve fitting with a combination of Gaussian and Lorenzian distributions. The three O 1*s* peaks at 528.5, 530.3, and 531.1 eV systematically depended on the film preparation parameters. The O 1*s* peak having a binding energy with a centroid at 530.3 eV is obtained only in the Xe-doped Y-Ba-Cu-O films; this peak arose as a result of oxygen reacting with xenon doped into the films. The oxygen composition dependence of the intensity of the O 1*s* peak at 529.5 eV was opposite of those of the 530.3 eV O 1*s* peak intensity. Thus there is an optimum annealing temperature and an optimum copper composition in the target to increase the amount of the superconducting Y-Ba-Cu-O having compressed *a*-*b* lattice planes and expanded *c* lattice planes. In the Xe-Y4 films the intensity of the O 1*s* peak at 528.5 eV increased with increasing annealing temperature. A similar annealing temperature dependence of XPS spectra was exhibited for the Xe-Y2 and Xe-Y6 films. The Xe-Y2, Xe-Y4, and Xe-Y6 films exhibit a Y_{3d} spectra, splitting into two peaks related to the Y $3d_{3/2}$ and Y $3d_{5/2}$ spin orbit having binding energies at 156.6 and 159.9 eV and the Ba $3d_{5/2}$ peak having a binding energy with a centroid at 779.10 eV.

Figure 4 shows the Xe $3d_{5/2}$ spectra vs annealing temperature graph for the Xe-Y4 films annealed at 100–500 °C for 24 h. A similar graph could be obtained for the other films. The Xe $3d_{5/2}$ peak is measured at a binding energy of 669 eV. The binding energy is lower than the well-known value of 672 eV for xenon. The difference of 3 eV in the Xe $3d_{5/2}$ peak energy is about four times larger than the value of 0.8 eV which differs between the O 1*s* peak energy at 529.5 eV for oxygen in the superconducting Y-Ba-Cu-O lattices and the O 1*s* peak energy at 530.3 eV arising due to the presence of xenon. This indicates that one xenon chemically combines with four oxygens XeO_4 (Ref. 10) as a xenon-oxygen compound was formed in the Xe-doped Y-Ba-Cu-O films. Xenon started to liberate from the films into the air during annealing at temperatures above 200 °C. The distribution of xenon become shallower with increasing annealing temperature. A large amount of xenon still remains in the surface region in the film annealed at 500 °C.

C. Resistivity and susceptibility

The graphs of the resistivity vs temperature, obtained using the four-point technique, for the Xe-Y6 films annealed at 100–500 °C for 24 h are shown in Fig. 5. The resistivities agreed with those obtained using the van der Pauw technique within $\pm 4\%$. The inset in this figure shows a linear scale resistivity vs temperature graph for the 200 °C-annealed

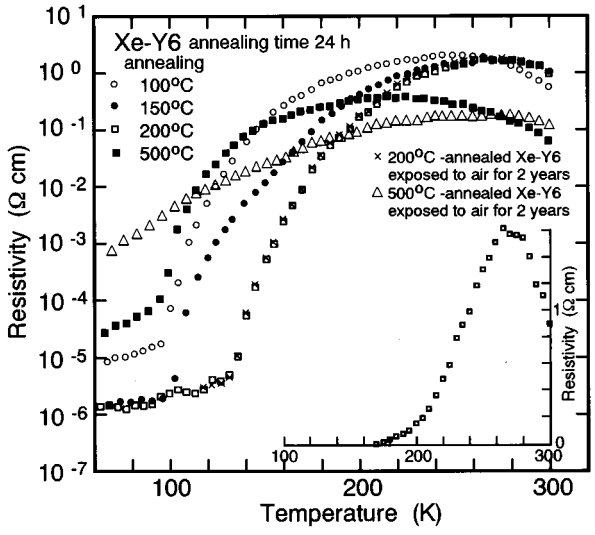

FIG. 5. The resistivity vs temperature graphs for the Xe-Y6 films annealed at 100–500 °C for 24 h.

TABLE IV. The magnetic susceptibility at 86.6 K for Xe-Y6 annealed in oxygen at 100–500 °C for 24 h.

Anneal temp.	$\Delta f(=\Delta f_S-\Delta f_X)$ (Hz)	$4\pi\chi$ (emu/cm^3)
100 °C	9.7 ± 2	-0.26 ± 0.26
150 °C	12.8 ± 2	-0.63 ± 0.15
200 °C	14.1 ± 2	-0.73 ± 0.11
500 °C	10.3 ± 2	-0.35 ± 0.23

Xe-Y6 films. The resistivities first increased with decreasing temperatures, exhibited a maximum value at 200–260 K, decreased exponentially, and reached very low residual resistivities at 95–130 K. The resistivity decrease was about five orders of magnitude around 90–200 K. The very low residual resistivity, however, was higher than $\pm5\times10^{-7}$ Ω cm, corresponding to the detection limit of the measurement. The films were further tested at lower temperatures, and the zero resistance of the films were found to occur at 30–70 K. The zero resistance was confirmed by the fact that the potential difference between the two electrodes was not changed when the electric current was changed. The films were tested over more than six thermal cyclings. The resistance transition was reproducibly measured on all the films. The crosses and triangles in this figure show the resistivity vs temperature graph for the 200 °C- and 500 °C-annealed Xe-Y6 films, respectively, that were exposed to air for two years. The long period exposed 200 °C-annealed Xe-Y6 film exhibited the same resistivity vs temperature graph as the as-prepared film. However, the long period exposed 500 °C-annealed Xe-Y6 film exhibited a degraded resistivity vs temperature graph, compared with the as-prepared film. These films had approximately the same XPS spectra as the as-prepared films; we could not determine an XPS signal peak energy shift due to the electrical degradation of the films because the energy resolution of the XPS apparatus used was lower, as described already.

Table IV shows $\Delta f(=\Delta fs-\Delta fx)$ and $4\pi\chi$ at 86.6 K, where Δfx is the frequency change when the film deposited silicon was located in the center of the air core copper coil and Δfs is the frequency change when only silicon with the same weight was located in the center of the coil. Collected temperature vs frequency change curves could not be measured since a dummy sample cannot be located in the vicinity of the sample to monitor the film temperature during the ac magnetic susceptibility measurement. For the Xe-Y6 films annealed at 100–500 °C for 24 h, the smaller the resistivity at 100 K becomes, the larger the value of χ. However, the χ values of all the films do not approach its limiting diamagnetic value of $1/4\pi$ as the small sample volume attains a superconducting state. The similar relationship between the resistivity at 100 K and the value of χ was measured on other Xe-doped Y-Ba-Cu-O films. The 200 °C-annealed Xe-Y6 films, having a larger value of χ, had a larger amount of oxygen in the superconducting Y-Ba-Cu-O lattice, which was obtained using the XPS simulation fitting. This is similar to other experimental results that T_c increases with increasing oxygen composition (charge carrier density).[11,12]

D. A consideration for electrical conduction

The superconducting Y-Ba-Cu-O lattice in the Xe-doped Y-Ba-Cu-O films have been compressed along the a and b axes and have been expanded along the c axis; positive uniaxial pressures perpendicular to the a and b axes were simultaneously applied. The increase in the c axis bond lengths can be expected to lead to an increase in the separation between the Cu-O chains. The increase in the Cu-O distance decreases the degree of the molecular orbital overlap and decreases the degree of charge transfer into the CuO_2 planes. As a result, the superconducting transition temperature decreased.[13]

On the other hand, Boolchand *et al.*[14] have claimed that in Y-Ba-Cu-O. The transition temperature T_c to superconducting state is strongly coupled to the orthorhombic distortion $(b\text{-}a)$. Substituting Gd for Y in the $Y_{1-x}Gd_xBa_2Cu_3O_7$ system increases the cell volume, decreases $(b\text{-}a)$, and slightly increases T_c.[15] The system Y-Ba-Cu-O exhibits opposite signs of dT_c/dp_a and dT_c/dp_b and $dT_c/d(b-a)=-104$ K/A using the uniaxial strain derivatives;[14,16] a large increase in T_c should be obtained by simultaneously applying a positive and negative uniaxial-pressure along the b and a axes, respectively. However, in $RBa_2Cu_4O_8$ ($R=$ Sm, Eu, Gd, Dy, Ho, and Er) materials, which have a double chain running along the b axis, T_c is also correlated to $(b-a)$, but the dependence is of the opposite sign: $dT_c/d(b-a)>0$.[17] These results demonstrate the complexity of these systems.

Here, we propose the following superconduction mechanism. The Xe-doped Y-Ba-Cu-O films had xenon reacting with four oxygens in the superconducting Y-Ba-Cu-O lattices. The $YBa_2Cu_3O_6$ lattices were not disturbed by doping the xenon. Orthorhombic Y-Ba-Cu-O differs from tetragonal Y-Ba-Cu-O on whether oxygen substitutes on the atomic position of $(\frac{1}{2},0,0)$. The xenon can possibly substitute at the atomic position of $(\frac{1}{2},0,0)$ in the orthorhombic Y-Ba-Cu-O lattices. Thus, xenon on the atomic position of $(\frac{1}{2},0,0)$ reacts with O(1) atoms and O(4) atoms in the superconducting Y-Ba-Cu-O lattices. The Cu(1) atoms, that have a broken chemical bond with the neighbor oxygen atoms by doping xenon, would act as an electron trap. This results in an increase in the degree of charge (hole) transfer from the chains to the planes. The charge transfer relieves the decrease in the charge transfer due to the increase in the separation between the Cu-O chains.

IV. CONCLUSIONS

Xe-doped $YBa_{1.5}Cu_{6.3}O_x$, Xe-doped $YBa_{1.5}Cu_{3.7}O_x$, and Xe-doped $YBa_{1.5}Cu_{2.2}O_x$ thin films were deposited on unheated (100)Si substrates by Xe ion-beam sputtering and were annealed in flowing oxygen at 100–500 °C for 24 h. The samples exhibited a resistance decrease of about five orders of magnitude around 90–160 K. The resistive transition was reproducibly measured on all samples. The resistance transition was stable and reproducible on all the films except the 500 °C-annealed films even after being exposed in air at room temperature for two years. The superconducting Y-Ba-Cu-O lattices in the Xe-doped Y-Ba-Cu-O films were

compressed along the *a* and *b* axes and expanded along the *c* axis by doping xenon. The resistance decrease shifted to higher temperatures with the *c*-axis bond length, increasing with annealing temperature.

ACKNOWLEDGMENT

This research was supported by a Grant-in-Aid for Scientific Research of Priority Areas of Kansai University.

[1] S. R. Ovshinsky, R. T. Young, D. D. Allred, G. Demaggio, and G. A. Van der Leeden, Phys. Rev. Lett. **58**, 2579 (1987).

[2] J. Narayan, V. N. Shukla, S. J. Lukasiewicz, N. Biunno, R. Singh, A. F. Schreiner, and S. J. Pennycook, Appl. Phys. Lett. **51**, 940 (1987).

[3] J. T. Chen, L. E. Wenger, C. J. Mcewan, and E. M. Logothetis, Phys. Rev. Lett. **58**, 1972 (1987).

[4] M. K. Wu, J. R. Ashbum, C. J. Torng, P. H. Hor, R. L. Meng, L. Gao, A. J. Huang, Y. Q. Wang, and C. W. Chu, Phys. Rev. Lett. **58**, 908 (1987).

[5] Q. Y. Ma, Chin-An Chang, and E. S. Yang, J. Appl. Phys. **69**, 7348 (1991).

[6] K. Hatanaka and K. Yokota (unpublished).

[7] D. J. Lichtenwalner, C. N. Soble II, R. R. Woolcott, Jr., O. Auciello, and A. I. Kingon, J. Appl. Phys. **70**, 6952 (1991).

[8] A. Gauzzi and D. Pavuna, Appl. Phys. Lett. **66**, 1836 (1995).

[9] Z. Iqbal, E. Leone, R. Chin, A. J. Signorelli, A. Bose, and H. Eckhardt, J. Mater. Res. **2**, 768 (1987).

[10] A. F. Wells, *Structural Inorganic Chemistry* (Clarendon, Oxford, 1975) p. 323.

[11] E. Kaldis, P. Fischer, A. W. Hewat, E. A. Hewat, J. Karpinski, and S. Rusiecki, Physica C **159**, 668 (1989).

[12] C. C. Almasan, S. H. Han, B. W. Lee, L. M. Paulius, M. B. Maple, B. W. Veal, J. W. Downey, A. P. Paulikas, Z. Fisk, and J. E. Schirber, Phys. Rev. Lett. **69**, 680 (1992).

[13] G. Baumgärtel, W. Hüber, and K. H. Bennemann, Phys. Rev. B **45**, 308 (1992).

[14] C. Meingast, O. Kraut, T. Wolf, H. Wühl, A. Erb, and G. Müller-Vogt, Phys. Rev. Lett. **67**, 1634 (1991).

[15] A. A. R. Fernades, J. Santamaria, S. L. Bud'ko, O. Nakamura, J. Guimpel, and I. Schuller, Phys. Rev. B **44**, 7601 (1991).

[16] O. Kraut, C. Meingast, G. Bräuchle, H. Claus, A. Erb, G. Müller-Vogt, and H. Wühl, Physica C **205**, 139 (1993).

[17] H. B. Liu, D. E. Morris, and A. P. B. Sinha, Phys. Rev. B **45**, 2438 (1992).